The formation processes and development characteristics of boulder bars due to outburst flood triggered by the overtopped landslide dam failure

Xiangang Jiang✉[1] · Haiguang Cheng[1] · Lei Gao[2] · Weiming Liu[3]

[1]College of Civil Engineering, Sichuan Agricultural University, Dujiangyan, Chengdu 611830, China

[2]Key Laboratory of Ministry of Education for Geomechanics and Embankment Engineering, Hohai University, Nanjing 210098, China

[3]Key Laboratory of Mountain Hazards and Earth Surface Process, Institute of Mountain Hazards and Environment, Chinese Academy of Sciences, Chengdu 610041, China

Correspondence to: Xiangang Jiang (✉E-mail: jxgjim@163.com)

Abstract

Boulder bars are a common form of riverbed morphology that could be affected by landslide dams. However, few studies have focused on the formation processes and development characteristics of boulder bars triggered by outburst floods. In such way, eight group landslide dam failure experiments with movable bed length for 4 to 7 times of dam length are carried out to study the temporal and spatial distributions of 25 boulder bars along the riverbeds, the boulder bar geometric characteristics, and the influence of dam volume and the released flood volume on the total volume of boulder bars. The results show that boulder bars are formed after peak discharge of outburst flow. The number of boulder bars is 0.4 to 1.0 times the ratio of river bed length to dam length. Besides, boulder bars have the characteristic of lengthening towards upstream

during the failure process. Boulder bar's upstream edge has a more extensive development than boulder bar downstream edge. The length of a boulder bar along the channel changes faster than the boulder bar's width and height. The boulder bar's length is about 7 to 16 times of width. The landslide dam can provide materials for the formation and development of the boulder bar. When landslide dam volume is larger, the boulder bars' total volume on the river bed is larger. Specifically, when the released flood volume is larger, the boulder bars' total volume will be larger. Comparing the experimental results in this paper with the Yigong field data, many characteristics of the experiments and the field are consistent. Therefore, results in this paper can be applied to the river channel's geomorphological characteristics analysis triggered by overtopped landslide dam failure.

Keywords

Landslide dam · Overtopping failure · Dam volume and released flood volume · boulder bar formation and development

1. Introduction

Activities such as rainfalls and earthquakes often cause landslides, which block the river to form a water-retaining body similar to a reservoir dam, called a landslide dam (Takahashi, 2007; Costa and Schuster, 1988; Casagli, 2003). According to statistics, 85 % of the dams failed within one year after formations, and more than 50 % of the dams breach with overtopping mode (Costa and Schuster, 1988). When the dam breach, the storage water erupt and flow to the downstream riverbed.

Many studies on the influence of flood geomorphology and sedimentary characteristics have proved that the outburst flood energy is huge, and it can entrain and transport materials of various sizes, from clay to boulders. A large number of boulders gather in the river to form bars, namely boulder bars. The downstream riverbed's geomorphology will be significantly affected and undergo significant changes (Lamb and Fonstad, 2010; Maizels, 1997; Russell and Knudsen, 1999; Marren and Schuh, 2009; Benito and O'Connor, 2003; Carling, 2013; Wu et al., 2020). Boulder bars are one common landform formed during the outburst flood evolution (Turzewski et al., 2019; Jiang and Wei, 2020; Wu et al., 2020). For example, in the 2000 year, Yigong outburst flood, due to its huge lake storage, formed many huge boulder bars on the river bed. The boulder bars had a significant impact on the development of the river. And Wu et al. (2020) investigated the impact of this event on river morphology and analyzed the shapes and geometric characteristics of the boulder bars caused by the overtopping flood. And they found that the boulder bar components are poorly sorted. Turzewski et al. (2019) studied the particle gradation of the boulder bars during the Yigong River landslide dam failure process. They found that the boulder bars' particle sizes decrease along the lower reaches of the river bed. But they did not analyze the evolution characteristics of boulder bar's size in detail. Lamb and Fonstad (2010) suggested that the rising and falling stages of the outburst flood had a greater impact on riverbed geomorphology and analyzed the characteristics of the median diameter of material in boulder bar.

Because lack of field investigations about the growth characteristics of boulder

bars during the landslide dam failure process in the field, some researchers had conducted landslide dam failure experiments in the lab (Jiang and Wei, 2020; Ashworth, 1996). Ashworth (1996) used flume experiments to study the boulder bar's growth. However, in their experiment, the inflow conditions are quite different from the outburst flood. Therefore, the research results' applicability to the boulder bar formed by the outburst flood remains uncertain. Jiang and Wei (2020) qualitatively analyzed the formation process of boulder bar in the evolution of overtopping outburst floods using dam failure experiments and initially discussed the characteristics of geometric dimensions of boulder bars after dam failure. However, the characteristics of the boulder bar's positions and geometric sizes during the dam failure process have not been analyzed.

Above all, no matter whether it is field observations or indoor experiments, the boulder bar's development characteristic during the landslide dam overtopping failure process has not been proved. This paper focuses on the formation processes, the geometrical size characteristics of boulder bars in the downstream channel during the overtopping failure process, and how the dam volume and the released flood volume affect boulder bars' total volume. Firstly, through flume experiments, boulder bars' formation processes on the downstream channel under the dammed lake failure condition were reproduced. Then, based on the experimental data, the development characteristics of boulder bars' upstream and downstream edges were analyzed. Furthermore, statistical analysis of boulder bars geometrical dimensions at each moment during the failure process, such as length, width, height, and volume, had been

carried out to obtain boulder bars' size characteristics. And then, by analyzing the total volume of the boulder bar under different dam volumes and the released flood volumes, the influences of the released flood volume and dam volume on the boulder bar total volume were obtained. Finally, compare the boulder bar formed by the Yigong outburst flood and the boulder bar formed by the experiment to verify this experiment's reliability.

2. Experimental design

2.1 Model design and experimental materials

The longitudinal profiles of experimental landslide dams were trapezoidal and triangular. The trapezoidal dam height and crest width were both 0.3 m, and the triangular dam height was also 0.3 m. In the experiment, river bed slope angle θ was fixed at 10°, and the landslide dam upstream slope angle α was set to 40°, and the landslide dam downstream slope angles β were set to five different values. The moveable bed was set downstream of the model dam, which had a length of 8 m. The downstream channel bed's length was about 4 to 7 times of dam length along the channel. The test parameters are shown in Table 1.

Table 1 test parameters

No.	Dam shape	β (°)
T1	Trapezoid	10
T2	Trapezoid	15
T3	Trapezoid	20
T4	Trapezoid	25
T5	Trapezoid	30
T6	Tringle	10
T7	Tringle	15
T8	Tringle	20

Peng and Zhang (2012) proposed that landslide dam height (H_d), dam bottom width parallel to the channel (W_d), dam volume (V_d), and reservoir volume (V_l) are the key geometric parameters of landslide dam, and proposed a set of dimensionless numbers, $\frac{H_d}{W_d}$, $\frac{V_d^{1/3}}{H_d}$ and $\frac{V_l^{1/3}}{H_d}$, to verify whether the established dam model is consistent with the landslide dam in the field (Zhou et al., 2019). As the field data show that the $\frac{H_d}{W_d}$, $\frac{V_d^{1/3}}{H_d}$ and $\frac{V_l^{1/3}}{H_d}$ are ranged about 0.001 to 2, 0 to 40, and 0 to 20 for filed landslide dam (Zhou et al., 2019). Table 2 shows the dimensionless numbers of the experimental dams, which are all within the acceptable range of the field landslide dams, indicating that the dams in the experiments are relatively close to field landslide dams.

Table 2 landslide dam parameters. The value of $\frac{H_d}{W_d}$ ranges from 0.1 to 0.3, and $\frac{V_d^{1/3}}{H_d}$ and $\frac{V_l^{1/3}}{H_d}$ both range from 1 to 2, which all fall within the acceptable range of values of the field landslide dams (Zhou et al., 2019).

No.	H_d (m)	W_d (m)	$\frac{H_d}{W_d}$	$\frac{V_d^{1/3}}{H_d}$	$\frac{V_l^{1/3}}{H_d}$
T1	0.3	2.359	0.127	1.643	1.477
T2	0.3	1.777	0.169	1.513	1.477
T3	0.3	1.482	0.202	1.437	1.477
T4	0.3	1.301	0.231	1.387	1.477
T5	0.3	1.177	0.255	1.350	1.477
T6	0.3	2.059	0.146	1.508	1.477
T7	0.3	1.477	0.203	1.350	1.477
T8	0.3	1.182	0.254	1.254	1.477

The dam materials used in this study were mixtures of sand and gravels, with a median particle size D_{50} of 3.8 mm. Due to the flume space limitation, the maximum sediment particle size was set to 20 mm. The riverbed was movable, which consisted of the same material as the dam model. The thickness of the riverbed was set to 0.06 m. The gradation curve of material particles' sizes is shown in Fig. 1.

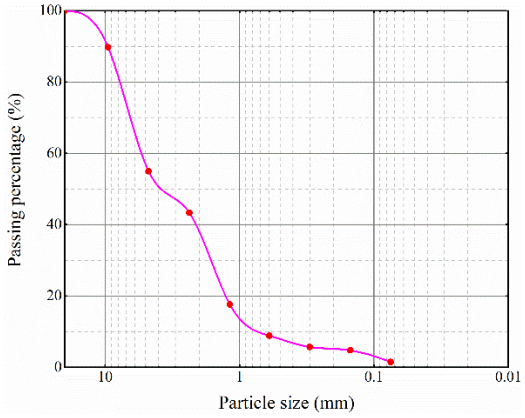

Figure. 1 Gradation curve of the dam materials

2.2 Experimental apparatus

The experimental setups are shown in Fig. 2. The flume was 15 m long, 0.3 m wide, and 0.6 m high. The flume slope was adjustable from 10 to 30°. One side of the flume was transparent glass, and scale lines were drawn on the glass to facilitate observation and recording of experimental phenomena. The inflow discharge was set as 1.0 L s^{-1}. Under the control of the electromagnetic flowmeter, the error range could be controlled within ±0.01 L s^{-1}. In addition, piezometers were embedded at the toe of the dam upstream slope, which can help calculate the failure discharge. During the tests, the toe of the dam upstream slope was set at 4.5 m away from the water supply tank. A baffle with a height of 6 cm was set at the flume end as a boundary condition. Seven cameras were placed on the transparent glass side of the flume, one camera was placed on the top of the dam, and one camera was placed directly behind the flume. A total of nine cameras recorded the whole experimental phenomena.

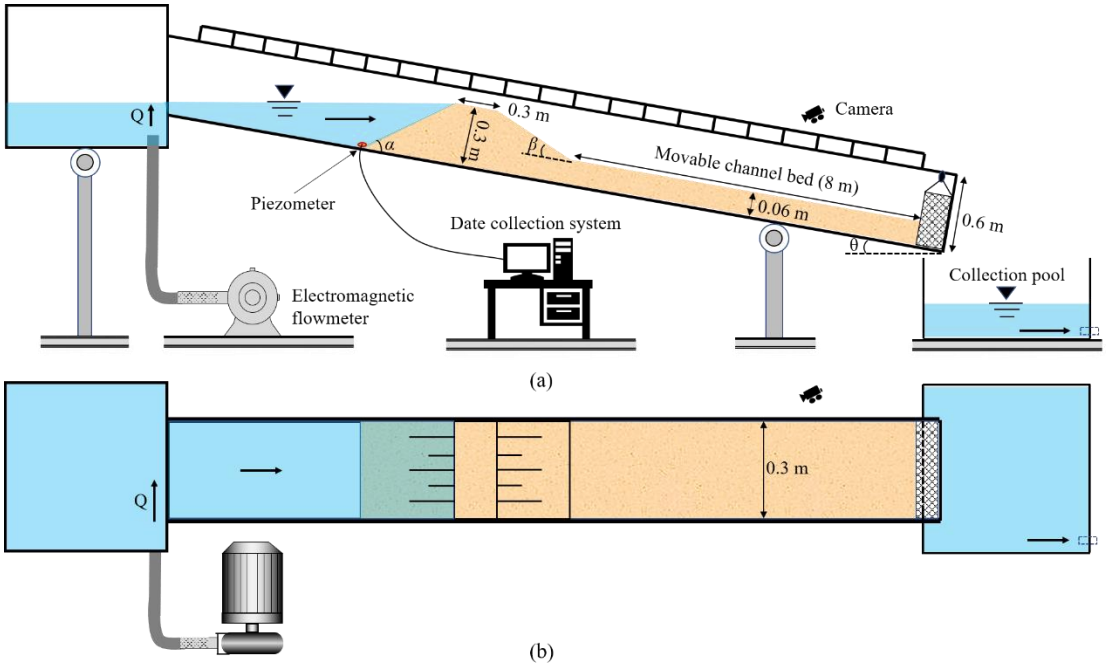

Figure. 2 Experimental setups. (a) Front view of the flume. (b) Top view of the flume.

2.3 Measurements

In the experiment, using the scale lines on the transparent glass on the side of the flume, we can accurately read the boulder bars' positions at each moment. Boulder bars' lengths, widths, and heights could be obtained from the screen. The boulder bars formed in their experiment were irregular, and the boulder bars' height close to the flume wall were slightly different from the height at other positions (Chen et al., 2015; Jiang and Wei, 2020). Therefore, in this experiment, we selected the boulder bars' section along the flume wall as concerned positions. And we took the average height or width along the wall of the flume as the representative height or width values of the boulder bars. According to the actual boulder bars' geometric characteristics, the boulder bars were divided into several parts, and then the volume calculation formula of the similar geometric body was used to calculate the volume of each part respectively, and finally, the boulder bars' volumes were obtained by summing.

According to the principle of hydrostatic pressure, the piezometers in front of the dam can record the real-time changes of the water level. The water volume in front of the dam can be obtained through the water level in front of the dam and the geometric dimensions of the dam model:

$$V_{(t)} = \frac{1}{2} h_{(t)}^2 [\cot\theta + \cot(\alpha - \theta)] d * 1000 \quad (1)$$

where t is the time, s; $V_{(t)}$ is the water volume in front of the dam at time t, L; $h_{(t)}$ is the height of the water surface in front of the dam at time t, m; α is landslide dam upstream slope angle, °; θ is river bed slope angle, °; d is the width of the flume, m.

According to the water balance equation, the overtopping discharge can be obtained as:

$$Q_{out} = Q_{in} - \frac{dV}{dt} \quad (2)$$

in which Q_{out} is the breaching discharge at the breach, L s^{-1}; Q_{in} is the inflow rate L s^{-1}. Equation (2) can be used to obtain the breaching discharge at each moment, and then the volume of released flood in the dam failure process can be obtained.

3. Experimental results

3.1 Formation processes of boulder bars

The formation processes of boulder bars are almost similar for all the tests. Therefore, it takes the T7 test as an example to analyze below in this section, as shown in Fig. 3. When the flow overtopped the dam crest, the outburst flood carried the dam materials to the dam downstream slope (T=5 s) and then to the channel bed (T=19 s) with outburst flow discharge increasing. It should be noted that although a large number

171 of sediments were transported on the channel bed before the peak discharge, no boulder
172 bar formed on the downstream channel bed. After the moment of peak discharge, the
173 flow discharge gradually weakened, and dam materials were transported to the position
174 near the dam toe. The flow could not transport all the sediments away, and some
175 sediments gradually silted down, then the first boulder bar occurred near the dam toe
176 (T=30 s, the boulder bar in the figure is marked with a blue dotted line). After the first
177 boulder bar was formed, the flow direction was changed when water flow bypassed the
178 boulder bar. And the moving sediments still moved along the original direction due to
179 inertia, which causes sediments piled up to form the second boulder bar on the opposite
180 side of the first boulder bar (T=33s).

181 Similarly, the first and second boulder bars affected the formation of the boulder
182 bar downstream. Eventually, boulder bars were scattered on both sides of the channel,
183 forming a meandering channel downstream (T=40 and 47 s). This phenomenon is in
184 good agreement with the field boulder bars along the Yigong river (Wu et al., 2020).

185

186 **Figure. 3** The riverbed morphology at six different moments during the boulder bars' formations
187 and growths process for the T7 experiment. The boulder bars in the figure are marked with blue
188 dotted lines.

3.2 Characteristics of the boulder bars' positions

Figure. 4 shows boulder bars' locations on the channel bed during the dam failure process. The red lines in the figure represent the boulder bars' outlines, and the orange rectangles represent the channels. It clearly shows the formation sequences of boulder bars at different locations. That is, boulder bars were formed first near the dams (upstream reaches of riverbed), and the farther from the dam toe, the later the boulder bar was formed, which is consistent with the content of Sect. 3.1. Boulder bars near the downstream dam toes are all located on the dam breach side across the river. This characteristic has also been found in Chen et al. (2015).

According to the boulder bars' formation sequences, the channel bed's boulder bars were divided into three types: I. the boulder bar near the upstream reaches, that is, the boulder bar near the dam toe; II. the boulder bar at the middle reaches; and III. the boulder bar near the downstream reaches. Figure 4 shows that the upstream edges of the boulder bars of type I for all the tests basically moved toward the dams with time development. The movement directions of the downstream edges of boulder bars of type I showed a little different: for T1, T2 and T5, the boulder bars' downstream edges moved toward the dam toes, from a distance from the downstream toe of 3.6 to 2.55 m, 3.3 to 2.9 m and 3.7 to 3.4 m, respectively, as shown in Fig.4 (a), (b) and (e); for T6, T7, and T8, the boulder bars' downstream edges first moved away from the dam toes and then moved toward the dam toes, and the downstream edges move forward compared to the original location. However, the distance they moved is 0.1 to 0.2 m, as shown in Fig.4 (f), (g), and (h); for T3 and T4, the boulder bars' downstream edges

positions remained almost unchanged, see Fig. 4(c) and (d). No matter how the downstream edge positions of the boulder bars type I changed, there is a common feature: compared with the initial positions of the boulder bars, the downstream edges almost remained original locations, and the movement distances were much smaller than those of boulder bars' upstream edges. The lengths of the boulder bars of type I increased with the failure time. It can be seen that the sediments on the boulder bars' upstream edges played a great role in the length developments of type I boulder bars.

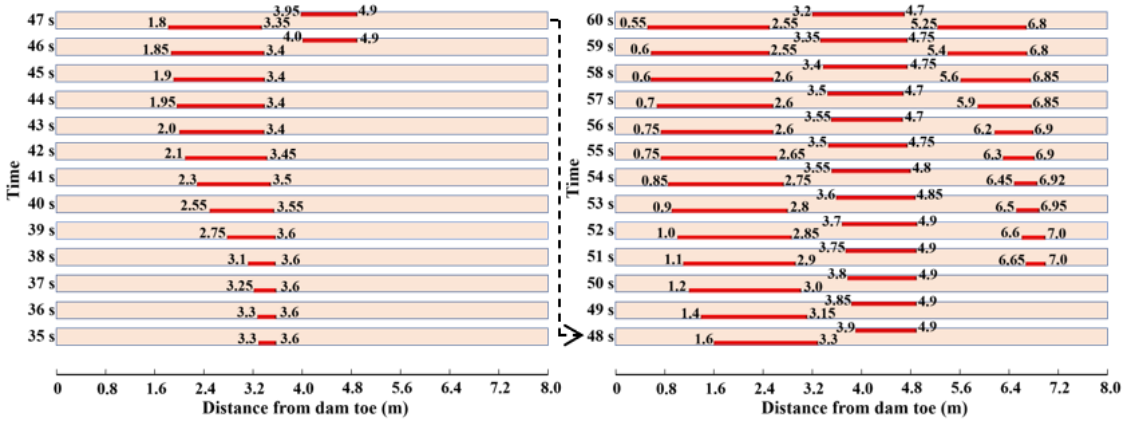

(a)

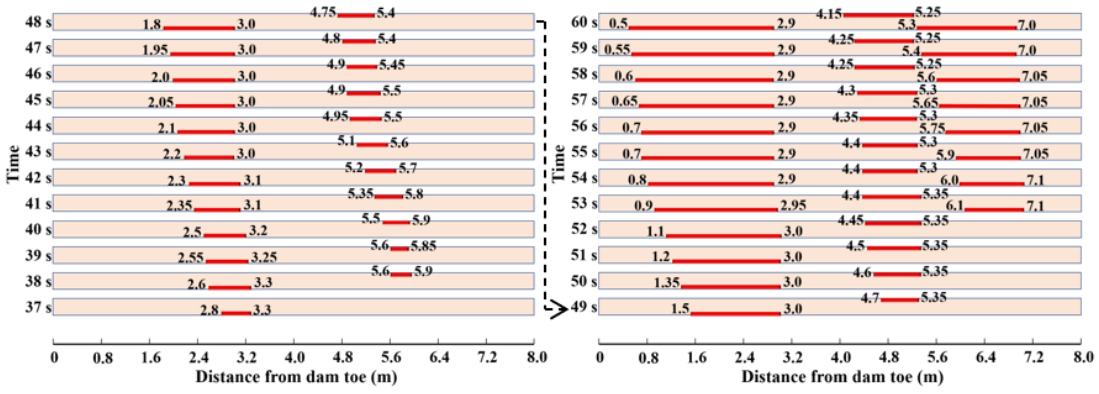

(b)

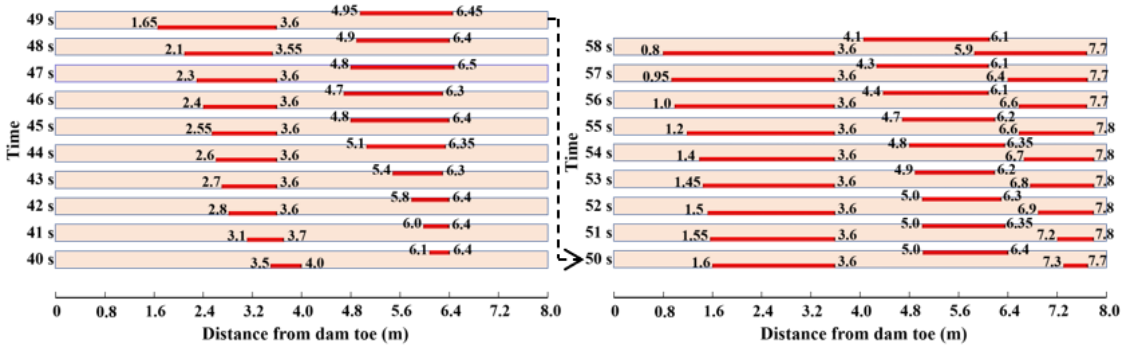
Time
Distance from dam toe (m)
0 0.8 1.6 2.4 3.2 4.0 4.8 5.6 6.4 7.2 8.0

(c)

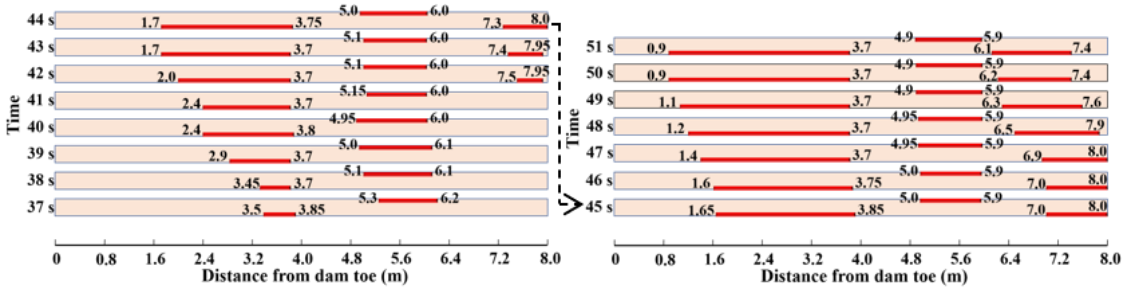
Time
Distance from dam toe (m)
0 0.8 1.6 2.4 3.2 4.0 4.8 5.6 6.4 7.2 8.0

(d)

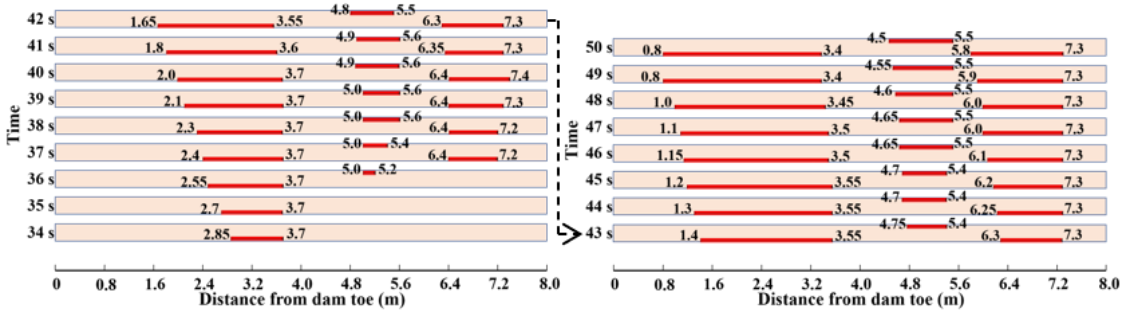
Time
Distance from dam toe (m)
0 0.8 1.6 2.4 3.2 4.0 4.8 5.6 6.4 7.2 8.0

(e)

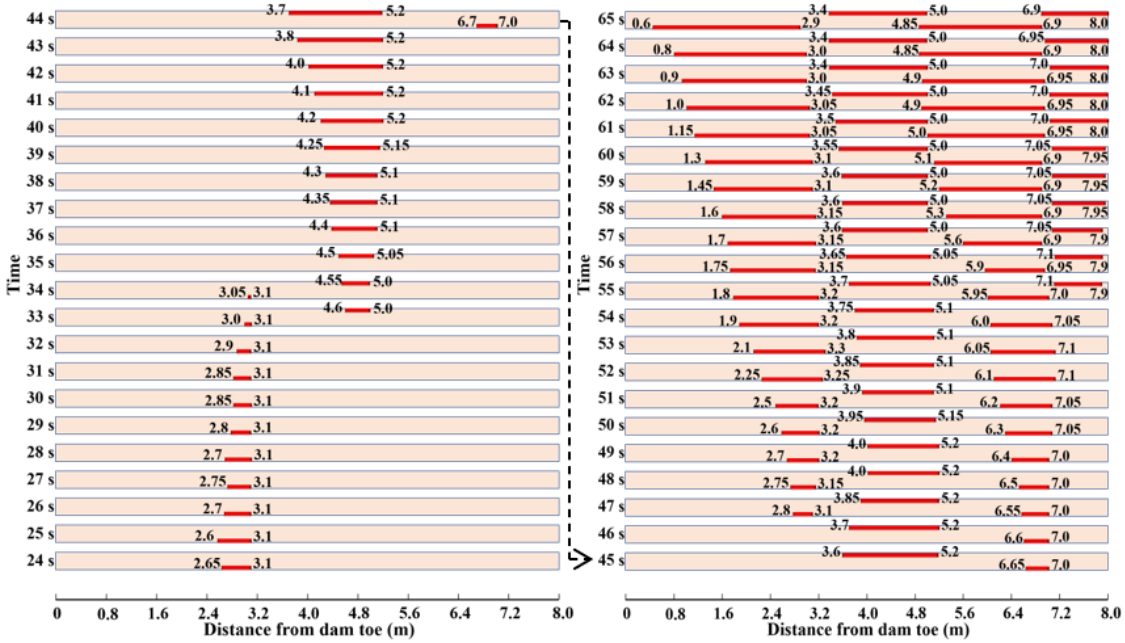
Time
Distance from dam toe (m)
0 0.8 1.6 2.4 3.2 4.0 4.8 5.6 6.4 7.2 8.0

(f)

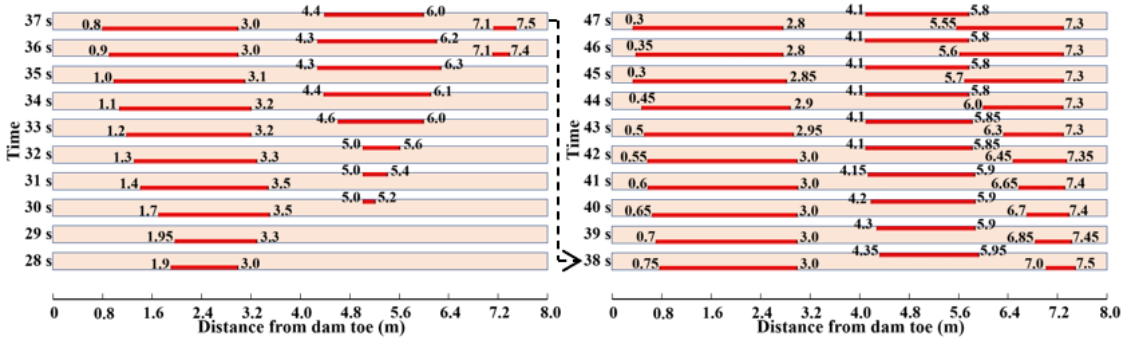

(g)

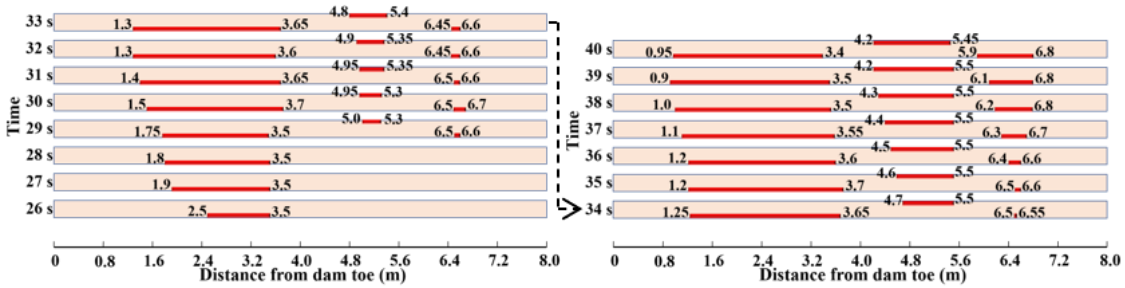

(h)

Figure. 4 The boulder bars' locations during the dam failure process. Notation: (a) to (h) represent the boulder bars' locations for T1-T8 tests, respectively. The red lines in the figure represent the boulder bars, and the orange rectangles represent the channels. The numbers at both ends of the red lines represent the distances between the upstream and downstream edges of boulder bars and the dam toe.

The positions of the upstream edges of type II and III boulder bar moved toward the dam toe during dam failure, but the downstream edges' positions could move toward or away from the dam. The distances of movement of the downstream edge positions were smaller than that of upstream edge positions. Compared with the boulder bars of type I, the movements of type II and III boulder bars were smaller. The distance between the boulder bars in the middle and downstream reaches is smaller than the distance between boulder bars near the upstream reaches and adjacent boulder bars.

3.3 Characteristics of the boulder bars' geometric sizes

It is corresponding to Sect. 3.2, Fig. 5 shows that the lengths of the boulder bars of type I were longer than other types of boulder bars' lengths due to the sufficient incoming materials from the upstream dam. For all the boulder bars, their lengths along the channel were largest, followed by widths, and lastly the heights. Boulder bars' lengths had a growing trend, and their growth rates were larger than widths and heights.

The boulder bars' shapes were irregular during the entire dam failure process, similar to the field boulder bars (Wu et al., 2020). The average values of the widths and heights of the boulder bars along the channel were selected as the parameters reflecting the characteristics of boulder bars' widths and heights (Fig. 5). The figure shows that boulder bars' heights changed less drastically than widths, which because boulder bars' heights were significantly affected by outburst flow depth. In most cases, flow depth was less than the heights of boulder bars. The sediments mainly accumulated at the boulder bars' edges and waists and could not "climb up" boulder bars' tops. Besides, the reduction of flow depth was not large enough, so the boulder bars' heights did not change seriously. The boulder bars' widths were significantly affected by the discharge of the outburst flow. When the discharge was enough, the sediments around the boulder bars were taken away by the flow, and the widths decreased. The variations of widths and heights both increase slowly with time and then tended to be stable values.

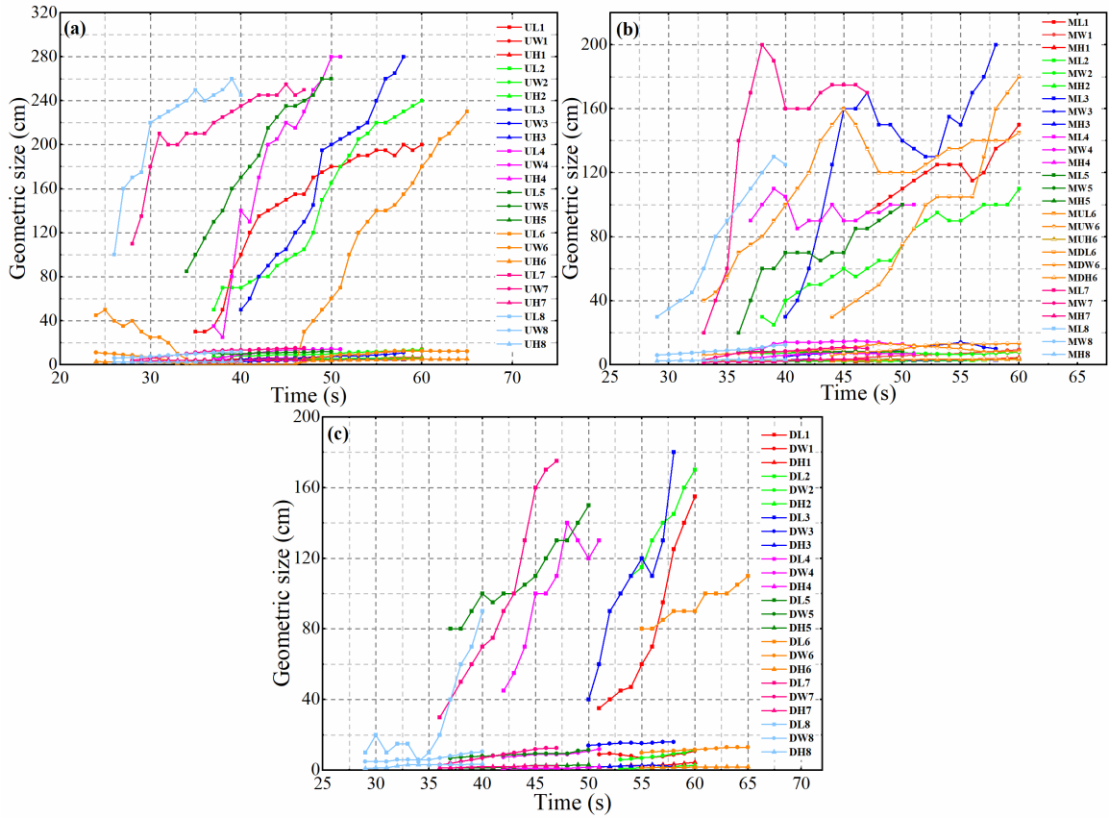

Figure. 5 The lengths, widths, and heights of the boulder bars: (a) sizes of the boulder bars near the upstream reaches; (b) sizes of the boulder bars near the middle reaches; (c) sizes of the boulder bars near the downstream reaches. Notation: L, W, and H represent the length, width, and height of the boulder bar, respectively. i represents the Ti experiment. For example, MUL6 indicates the length of the boulder bar near the middle-upstream reaches for the T1 test.

When the amounts of sediments deposited on boulder bars were larger than the quantities of eroded sediments, boulder bars' volumes became larger. Otherwise, boulder bars' volumes would decrease or remain at a stable level. Figure. 6 reveals boulder bars' volume characteristic during the dam failure. Most of the 25 boulder bars gradually increased in volume, indicating that the amounts of outburst flow erosions in the boulder bars' vicinities were less than the amounts of siltation during the entire outburst process. Referred to Figs. 5 and 6, the boulder bars' volume characteristics

were consistent with the boulder bars' length characteristics. And because the widths and heights developed slightly, boulder bars' volumes were mainly controlled by boulder bars' lengths.

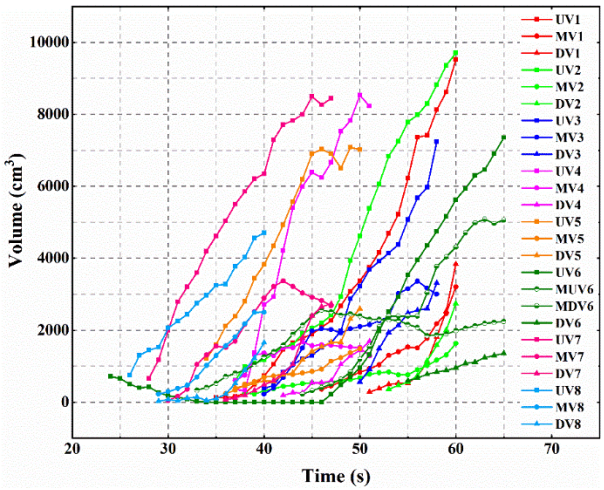

Figure. 6 Volumes of boulder bars. Notation: UVi, MVi, DVi, MUVi, MDVi represent the volume of the boulder bar near the upstream reaches, the boulder bar near the middle reaches, the boulder bar near the downstream reaches, the boulder bar near the middle-upstream reaches, and the boulder bar near the middle-downstream reaches, respectively. For example, UV1 means the volume of the boulder bar near the upstream reaches of the T1 test.

4. Influences of the dam volume and the released flood volume on total boulder bar volume

The boulder bar's formation and development are inseparable from the combined action of outburst flow and sediment. The landslide dam can provide materials for the development of the boulder bar, while the outburst flow provides hydraulic conditions.

Figure. 7 shows the boulder bars' total volume on the river bed when the dam fully failed. It can be seen that the total volume of the boulder bars is much lower than the

dam volume. The volumes were about 0.079 to 0.127, 0.017 to 0.078, and 0.015 to 0.041 times of the initial dam volumes for the boulder bars near the upstream reaches, the boulder bars near the middle reaches, and the boulder bars near the downstream reaches, respectively. The ratio of the total volume of the boulder bars to the dam volume is 0.138 to 0.208. It shows that only a small part of the dam material participates in the boulder bar's formation and development. During the process, most of the dam material was taken away by the outburst flow. Moreover, when the dam volume decreases, the amount of sediment involved in the development of the boulder bar decreases. The total volume of the boulder bars on the river bed also shows a decreasing trend.

This experiment counted the released flood volume during the dam failure process, as shown in Fig. 8. It could be seen that the released flood volume in the dam failure process of the T1 to T8 experiments decreased. According to Figs. 7 and 8, it could be found that with the decrease of the released flood volume, the total volume of boulder bars on the river bed shows a decreasing trend. When the released flood volume is small in the dam failure process, a small amount of flood is not enough to transport many dam materials to the downstream riverbed. There is less sediment on the riverbed, and the deposit that can participate in the boulder bar's growth is less. Therefore, the total volume of the boulder bars on the river bed at the moment of complete dam failure decreased with the decrease of the released flood volume.

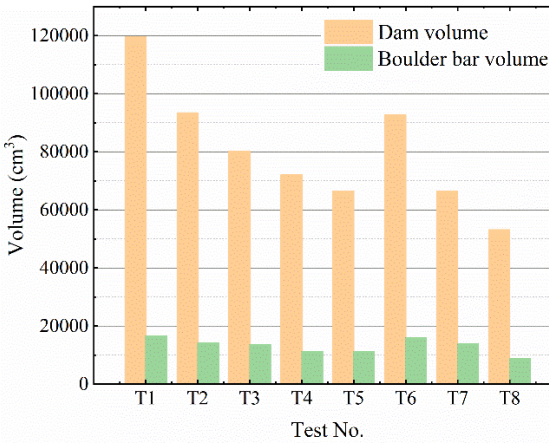

Figure. 7 The boulder bar's total volume and dam volume

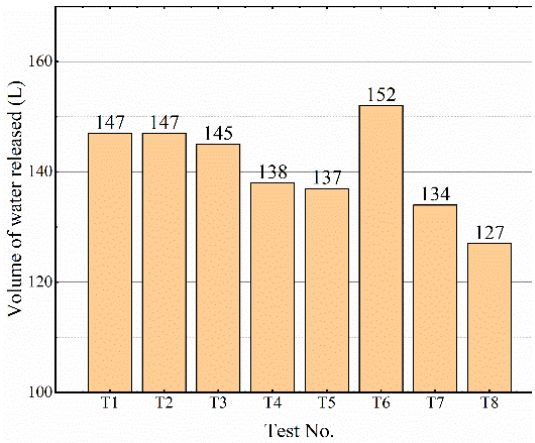

Figure. 8 The volume of water released during the dam failure.

5. Discussion

The field data of the Yigong landslide dam are used to verify the reliability of the results in this paper. Turzewski et al. (2019) investigated the boulder bars in the Yigong River triggered by the Yigong landslide dam outburst flood in 2000. They found that the number of boulder bars is about 0.69 to 0.77 times the ratio of river bed length to dam length for the boulder bar frequent region. In this study, boulder bars were distributed in the 8 m length of the channel, which is 4 to 7 times of dam length. It reflected the number of boulder bars was 0.4 to 1.0 times the ratio of river bed length to dam length. By comparing the experimental data and the field data of Turzewski et al. (2019), it can be found that field data falls within the range of experimental data. Experimental models took more influence factors into account in this paper, while the field data of Turzewski et al. (2019) only focused on the Yigong landslide dam case. This may be why the field data range is smaller than the experimental data in this paper.

Wu et al. (2020) classified the boulder bars in the downstream reaches of the

328 Yigong River into three types according to their shapes and used the length to width
329 ratio as the indicator of a bar shape. The 16 boulder bars in the downstream reaches of
330 the Yigong River have a length to width ratio of 2.5-15. As can be seen from Fig. 9, the
331 length to width ratio of the boulder bar formed in this experiment is in the range of 7 to
332 16, which indicates the field data could prove the experimental results.

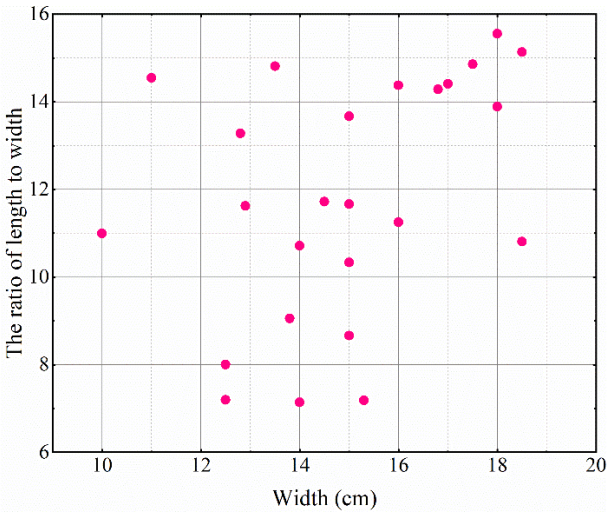

333
334 **Figure. 9** The ratio of boulder bar length to width

335 Turzewski et al. (2019) measured the sizes of boulder bars. They found that grain
336 sizes of boulder bars decrease downstream. In this experiment, boulder bar materials
337 from different river bed sections were collected. And after screening and analysis, it
338 was found that as the distance between the boulder bar and the dam increases, the
339 particle diameter in the bars shows a decreasing trend, as shown in Fig. 10. This feature
340 is consistent with the description of Turzewski et al. (2019).

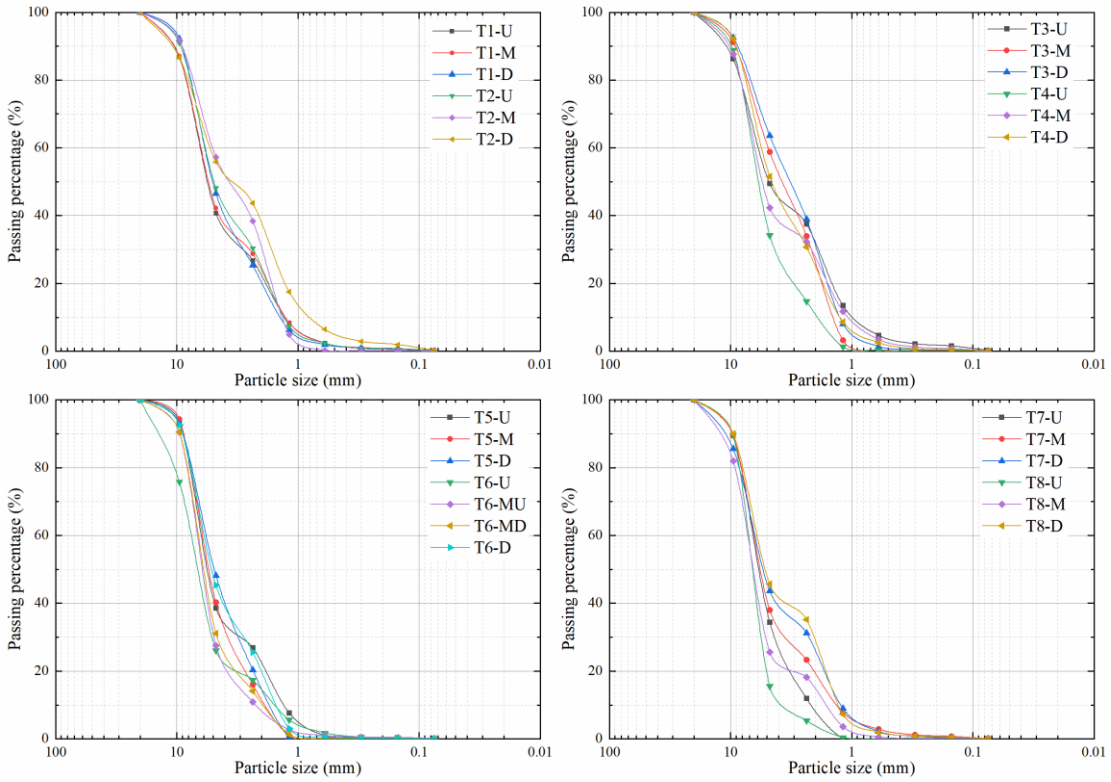

Figure. 10 Gradation curve of the boulder bar materials. Notation: U, M, D, MU, and MD, represent the boulder bar near the upstream reaches, the boulder bar near the middle reaches, the boulder bar near the downstream reaches, the boulder bar near the middle-upstream reaches, and the boulder bar near the middle-downstream reaches, respectively.

Based on the above points, it can be seen that the experimental results in this paper are consistent with the actual boulder bars in the field. Therefore, the experimental results can provide guidance for the field study of the boulder bar formed by the outburst flood.

6. Conclusion

In this paper, a downstream moveable bed for 4 to 7 times the length of landslide dam length along the channel was set, and through eight flume experiments, 25 boulder bars were formed downstream channel caused by overtopping flow. The boulder bars' development characteristics, the influences of dam volume and the released flood

volume on boulder bars were also analyzed. The main conclusions are as follows.

(1) Boulder bars first appear near dam toes (upstream reaches located on the dam's initial breach sides. Inertia force made sediment accumulate on the opposite banks of the channel bed, resulting in boulder bars' formations downstream. During the landslide dam failure process, the boulder bars' upstream edges are mainly in siltation states. The boulder bars' lengths increase with failure time, mainly caused by boulder bars' upstream edges move upstream. The downstream edges develop slowly and basically near the initial positions. And the developments of boulder bars' downstream edges are much smaller than the developments of boulder bars' upstream edges.

(2) During the dam failure process, the lengths varied faster than the widths and heights of boulder bars. And the boulder bars' lengths along the river are the largest, followed by widths, and lastly the heights when the dam completed failed. The volumes of the boulder bars increase with dam failure, and boulder bars' volume characteristics are consistent with boulder bars' lengths characteristics.

(3) After dam failure, the dam sediment is the material source for the development of the boulder bars, and the flow is the external driving force for the development of the boulder bar. When the dam volume is larger, more dam materials will be deposited on the river bed and participate in the boulder bar's growth, then the total boulder bar volume increases. When the released flood volume increases, the boulder bars' total volume on the river bed also increases.

(4) The experimental results are compared with Yigong outburst flood from three aspects: the ratio of the number of boulder bars on the river bed to the ratio of river bed

length to dam length, the ratio of boulder bar length to width, and the particle size of the boulder bar. The experimental results are in good agreement with the Yigong landslide dam case, which shows that the experimental results have certain reliability and can provide a reference for the field research of the boulder bar formed by the overtopping outburst flood.

Author contribution

Xiangang Jiang was responsible for the experiments, article thinking, and writing. Haiguang Cheng was responsible for calculating the article parameters. Lei Gao was responsible for the article's pictures, and Weiming Liu was responsible for checking the full article.

Competing interests

The authors declare that they have no known competing financial interests or personal relationships that could have appeared to influence the work reported in this paper.

Acknowledgments

This research has been supported by The National Natural Science Foundation of China (No. 41807289) and Key Laboratory of Ministry of Education for Geomechanics and Embankment Engineering, Hohai University (No. 202020) and Open fund of Key Laboratory of mountain hazards and surface processes, Chinese Academy of Sciences

(No. KLMHESP-20-05).

Code and data availability statement

The codes and data that support the findings of this study are available from the corresponding author upon reasonable request.

Reference

Ashworth, P. J.: Mid-channel bar growth and its relationship to local flow strength and direction, Earth Surf. Process. Landforms, 21, 103-123, https://doi.org/10.1002/(SICI)1096-9837(199602)21:2<103::AID-ESP569>3.0.CO;2-O, 1996.

Benito, G. and O'Connor, J. E.: Number and size of last glacial Missoula floods in the Columbia River valley between the Pesco Basin, Washington, and Portland, Oregon. Geological Society of America Bulletin, 115, 624 –638, https://doi.org/10.1130/0016-7606(2003)115<0624:NASOLM>2.0.CO;2, 2003.

Carling, P. A.: Freshwater megaflood sedimentation: what can we learn about generic processes? Earth-Science Reviews, 125, 87113, https://doi.org/10.1016/j.earscirev.2013.06.002, 2013.

Casagli, N., Ermini, L. and Rosati, G.: Determining grain size distribution of the material composing landslide dams in the Northern Apennines: Sampling and processing methods, Engineering Geology, 69, 83-97, https://doi.org/10.1016/S0013-7952(02)00249-1, 2003.

Chen, S. C., Lin, T. W. and Chen, C. Y.: Modeling of natural dam failure modes and

417 downstream riverbed morphological changes with different dam materials in a
418 flume test, Engineering Geology, 188, 148-158,
419 https://doi.org/10.1016/j.enggeo.2015.01.016, 2015.
420 Costa, J. E. and Schuster, R. L.: The formation and failure of natural dams, Geol Soc
421 Am Bull, 100(7), 1054-1068, https://doi.org/10.1130/0016-
422 7606(1988)100<1054:TFAFON>2.3.CO;2, 1988.
423 Jiang, X. G. and Wei, Y. W.: Erosion characteristics of outburst floods on channel beds
424 under the conditions of different natural dam downstream slope angles, Landslides,
425 1-12, https://doi.org/10.1007/s10346-020-01381-y, 2020.
426 Lamb, M. and Fonstad, M.: Rapid formation of a modern bedrock canyon by a single
427 flood event. Nature Geosci, 3, 477 –481, https://doi.org/10.1038/ngeo894, 2010.
428 Maizels, J. K.: Jökulhlaup deposits in proglacial areas. Quaternary Science Reviews,
429 16, 793 –819, https://doi.org/10.1016/S0277-3791(97)00023-1, 1997.
430 Marren, P. M. and Schuh, M.: Criteria for identifying jökulhlaup deposits in the
431 sedimentary record. In: Burr, D.M., Carling, P.A., Baker, V.R. (Eds.),
432 Megaflooding on Earth and Mars, Cambridge University Press, 225-242,
433 https://doi.org/10.1017/CBO9780511635632, 2009.
434 Peng, M. and Zhang, L. M.: Breaching parameters of landslide dams, Landslides, 9, 1,
435 13-31, https://doi.org/10.1029/2018WR024107, 2012.
436 Russell, A. J. and Knudsen, O.: Controls on the sedimentology of the November 1996
437 jökulhlaup deposits, Skeiðarársandur, Iceland. In: Smith, N.D., Rogers, J. (Eds.),
438 Fluvial sedimentology VI. Special Publication of the International Association of

439 Sedimentologists, 28, 315 –329, https://doi.org/10.1002/9781444304213.ch23,
440 1999.
441 Takahashi, T.: Debris flow Mechanics, Prediction and Countermeasures, Taylor and
442 Francis Group, 35-38, https://doi.org/10.1201/9780203946282, 2007.
443 Turzewski, M. D., Huntington, K. W. and LeVeque, R. J.: The Geomorphic Impact of
444 Outburst Floods: Integrating Observations and Numerical Simulations of the
445 2000 Yigong Flood, Eastern Himalaya. Journal of Geophysical Research: Earth
446 Surface 124, 1056-1079, https://doi.org/10.1029/2018JF004778, 2019.
447 Wu C. H., Hu, K. H., Liu, W. M., Wang, H., Hu, X. D., and Zhang, X. P.: Morpho-
448 sedimentary and stratigraphic characteristics of the 2000 Yigong River landslide
449 dam outburst flood deposits, eastern Tibetan Plateau, Geomorphology, 107293,
450 https://doi.org/10.1016/j.geomorph.2020.107293, 2020.
451 Zhou, G. G. D., Zhou, M. J., Shrestha, M. S., Song, D. R., Choi, C. E., Cui, K. F. E.,
452 Peng, M., Shi, Z. M., Zhu, X. H., and Chen, H. Y.: Experimental investigation on
453 the longitudinal evolution of landslide dam breaching and outburst floods,
454 Geomorphology, 334, 29-43, https://doi.org/10.1016/j.geomorph.2019.02.035,
455 2019.